7-2013

Magnetic Field Generation in a Jet-Sheath Plasma via the Kinetic Kelvin-Helmholtz Instability

K.-I. Nishikawa
Center for Space Plasma and Aeronomic Research, University of Alabama in Huntsville

P. Hardee
Department of Physics and Astronomy, The University of Alabama

B. Zhang
Department of Physics, University of Nevada

I. Dutan
Institute of Space Science, Atomistilor 409

M. Medvedev
Department of Physics and Astronomy, University of Kansas

See next page for additional authors

Follow this and additional works at: https://tigerprints.clemson.edu/physastro_pubs

Part of the Astrophysics and Astronomy Commons

Recommended Citation

Please use publisher's recommended citation.

Authors

K.-I. Nishikawa, P. Hardee, B. Zhang, I. Dutan, M. Medvedev, E. J. Choi, K. W. Min, J. Niemiec, Y. Mizuno, A Nordlund, J T. Frederiksen, H Sol, M Pohl, and Dieter H. Hartmann

Annales
Geophysicae

Magnetic field generation in a jet-sheath plasma via the kinetic Kelvin-Helmholtz instability

K.-I. Nishikawa[1], P. Hardee[2], B. Zhang[3], I. Duţan[4], M. Medvedev[5], E. J. Choi[6], K. W. Min[6], J. Niemiec[7], Y. Mizuno[8], A. Nordlund[9], J. T. Frederiksen[9], H. Sol[10], M. Pohl[11], and D. H. Hartmann[12]

[1]Center for Space Plasma and Aeronomic Research, University of Alabama in Huntsville, 320 Sparkman Drive, ZP12, Huntsville, AL 35805, USA
[2]Department of Physics and Astronomy, The University of Alabama, Tuscaloosa, AL 35487, USA
[3]Department of Physics, University of Nevada, Las Vegas, NV 89154, USA
[4]Institute of Space Science, Atomistilor 409, Bucharest-Magurele 077125, Romania
[5]Department of Physics and Astronomy, University of Kansas, KS 66045, USA
[6]Korea Advanced Institute of Science and Technology, Daejeon 305-701, South Korea
[7]Institute of Nuclear Physics PAN, ul. Radzikowskiego 152, 31-342 Kraków, Poland
[8]Institute of Astronomy, National Tsing-Hua University, Hsinchu, Taiwan 30013, Republic of China
[9]Niels Bohr Institute, University of Copenhagen, Juliane Maries Vej 30, 2100 Copenhagen Ø, Denmark
[10]LUTH, Observatore de Paris-Meudon, 5 place Jules Jansen, 92195 Meudon Cedex, France
[11]Institute of Physics and Astronomy, University of Potsdam, Karl-Liebknecht-Strasse 24/25, 14476 Potsdam-Golm, Germany
[12]Department of Physics and Astronomy, Clemson University, Clemson, SC 29634, USA

Correspondence to: K.-I. Nishikawa (ken-ichi.nishikawa@nasa.gov)

Abstract. We have investigated the generation of magnetic fields associated with velocity shear between an unmagnetized relativistic jet and an unmagnetized sheath plasma. We have examined the strong magnetic fields generated by kinetic shear (Kelvin–Helmholtz) instabilities. Compared to the previous studies using counter-streaming performed by Alves et al. (2012), the structure of the kinetic Kelvin–Helmholtz instability (KKHI) of our jet-sheath configuration is slightly different, even for the global evolution of the strong transverse magnetic field. In our simulations the major components of growing modes are the electric field E_z, perpendicular to the flow boundary, and the magnetic field B_y, transverse to the flow direction. After the B_y component is excited, an induced electric field E_x, parallel to the flow direction, becomes significant. However, other field components remain small. We find that the structure and growth rate of KKHI with mass ratios $m_i/m_e = 1836$ and $m_i/m_e = 20$ are similar. In our simulations saturation in the nonlinear stage is not as clear as in counter-streaming cases. The growth rate for a mildly-relativistic jet case ($\gamma_j = 1.5$) is larger than for a relativistic jet case ($\gamma_j = 15$).

Keywords. Solar physics, astrophysics, and astronomy (Energetic particles)

1 Introduction

Recent kinetic simulations have focused on magnetic field generation via electromagnetic plasma instabilities in unmagnetized flows without velocity shear. Three-dimensional (3-D) particle-in-cell (PIC) simulations of Weibel turbulence (Nishikawa et al., 2005, 2008, 2009a) have demonstrated sub-equipartition magnetic field generation.

Velocity shears also must be considered when studying particle acceleration scenarios, since these trigger the kinetic Kelvin–Helmholtz instability (KKHI). In particular the KKHI has been shown to lead to particle acceleration and magnetic field amplification in relativistic shear flows (Alves et al., 2012; Liang et al., 2013; Nishikawa et al., 2013).

Furthermore, a shear flow upstream of a shock can lead to density inhomogeneities via the Magnetohydrodynamics (MHD) Kelvin–Helmholtz instability (KHI), which may provide important scattering sites for particle acceleration.

In our simulations a relativistic jet plasma is surrounded by a sheath plasma (Nishikawa et al., 2013). This setup is similar to the setup of our RMHD simulations (Mizuno et al., 2007). In one of our simulations, the jet core has $v_{core} = 0.9978c$ ($\gamma_j = 15$) pointing in the positive x direction in the middle of the simulation box as in Alves et al. (2012). Unlike Alves et al. (2012) the upper and lower quarter of the simulation box contain a stationary, $v_{sheath} = 0$, sheath plasma as shown in Fig. 1a. Our setup allows for motion of the sheath plasma in the positive x direction.

Overall, this structure is similar in spirit, although not in scale, to that proposed for active galactic nuclei (AGN) relativistic jet cores surrounded by a slower moving sheath, and is also relevant to gamma-ray burst (GRB) jets. In particular, we note that this structure is also relevant to the "jet-in-a-jet" or "needles in a jet" scenarios (Giannios et al., 2009, and papers therein), which have been invoked to provide smaller scale high-speed structures within a much larger, more slowly moving AGN jet. Similar smaller scale structures within GRB jets are also conceivable.

This more realistic setup will allow us to compute synthetic spectra in the observer frame. As mentioned by Alves et al. (2012), in a non-counter-streaming or unequal density counter-streaming setup the growing KKHI will propagate with the flow. For GRB jets, the relativistic jet core is thought to have a much higher density relative to the external medium. On the other hand, for an AGN jet the relativistic core is thought to be less dense than the surrounding sheath.

Recently the KKHI was investigated using a counter-streaming velocity shear setup for subrelativistic $\gamma_0 = 1.02$ and relativistic $\gamma_0 = 3$ cases (Alves et al., 2012). The shear flow initial condition was set by a velocity field with v_0 pointing in the positive x_1 direction, in the upper and lower quarters of the simulation box, and a symmetric velocity field with $-v_0$ pointing in the negative x_1 direction, in the middle-half of the box. Initially, the systems were charge and current neutral. In the subrelativistic case the simulation box dimensions were $20 \times 20 \times 20(c/\omega_p)^3$, where $\omega_p = (4\pi ne^2/m_e)^{1/2}$ is the plasma frequency, and they used 20 cells per electron skin depth (c/ω_p). The simulation box dimensions for the relativistic scenario were $250 \times 80 \times 80(c/\omega_p)^3$, with a resolution of 4 cells per (c/ω_p). Periodic boundary conditions were imposed in every direction.

Alves et al. (2012) found that KKHI modulations are less noticeable in the relativistic regime because they are masked by a strong DC magnetic field component (negligible in the subrelativistic regime) with a magnitude greater than the AC component. As the amplitude of the KKHI modulations grows the electrons from one flow cross the shear surfaces and enter the counter-streaming flow. In their simulations the protons being heavier ($m_p/m_e = 1836$) are unperturbed.

DC current sheets which point in the direction of the proton velocity form around the shear surfaces. These DC current sheets induce a DC component in the magnetic field. The DC magnetic field is dominant in the relativistic scenario because a higher DC current is set up by the crossing of electrons with a larger initial flow velocity and also because the growth rate of the AC dynamics is lower by $\gamma_0^{3/2}$ compared with a subrelativistic case (Alves et al., 2013). It is very important to note that this DC magnetic field is not captured in MHD (e.g., Zhang et al., 2009) or fluid theories because it results from intrinsically kinetic phenomena. Furthermore, since the DC field is stronger than the AC field, a kinetic treatment is clearly required in order to fully capture the field structure generated in unmagnetized or weakly magnetized relativistic flows with velocity shear. This characteristic field structure will also lead to a distinct radiation signature (Sironi and Spitkovsky, 2009; Martins et al., 2009; Frederiksen et al., 2010; Nishikawa et al., 2009b, 2010, 2011, 2012).

We previously reported results from our first simulations for a core-sheath case with $\gamma_j = 15$ and $m_i/m_e = 20$ (Nishikawa et al., 2013). Here we report new simulation results using the real mass ratio $m_i/m_e = 1836$. We find some differences from previous counter-streaming cases.

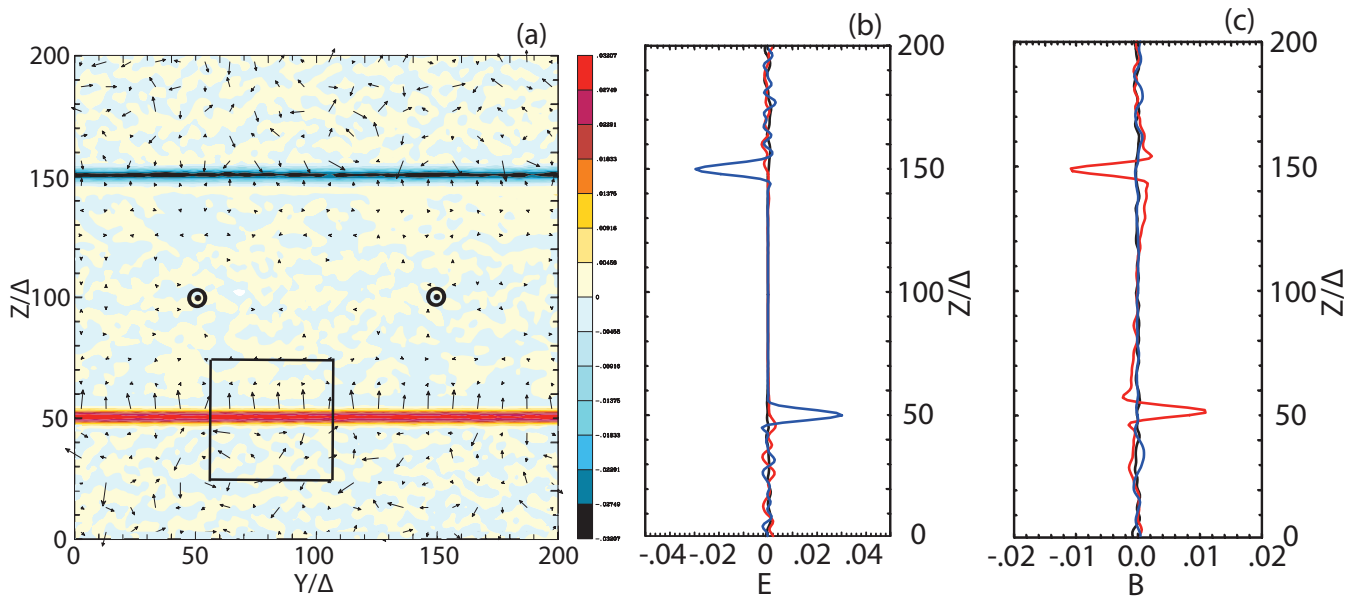## 2 Magnetic and electric field generation by KKHI

2.1 Initial core-sheath jet conditions

In this simulation study we investigate velocity shear in a core-sheath jet instead of the counter-streaming jets used in previous simulations (Alves et al., 2012; Liang et al., 2013). In this RPIC simulation the velocity shear occurs at the edges of a velocity field with v_{core} pointing in the positive x direction in the middle of the simulation box, with upper and lower quarters of the simulation box containing a velocity field with v_{sheath} pointing in the positive x direction as indicated by the arrows in Fig. 1a. Initially, the system is charge and current neutral.

We have performed a simulation using a system with $(L_x, L_y, L_z) = (1005\Delta, 205\Delta, 205\Delta)$ and with an ion to electron mass ratio of $m_i/m_e = 1836$ (Δ is the cell size). The jet and sheath plasma density is $n_{jt} = n_{am} = 8$. The electron skin depth, $\lambda_s = c/\omega_{pe} = 12.2\Delta$, where $\omega_{pe} = (e^2 n_a/\epsilon_0 m_e)^{1/2}$ is the electron plasma frequency and the electron Debye length λ_D is 1.2Δ. The jet Lorentz factor is $\gamma_j = 15$. The jet-electron thermal velocity is $v_{j,th,e} = 0.014\,c$ in the jet reference frame, where c is the speed of light. The electron/ion thermal velocity in the ambient plasma is $v_{a,th,e} = 0.03\,c$. Ion thermal velocities are smaller by $(m_i/m_e)^{1/2}$. We use periodic boundary conditions on all boundaries (Buneman, 1993; Nishkawa et al., 2009a, b).
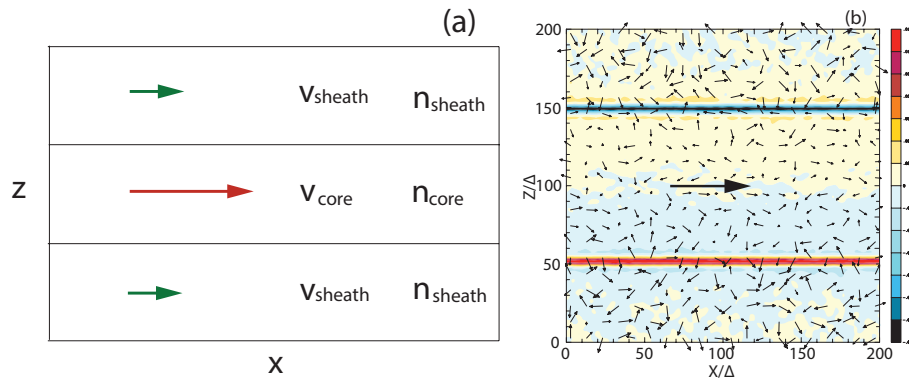
Fig. 1. Panel **(a)** shows our simulation model where the sheath plasma can be stationary or moving in the same direction as the jet core. In this simulation the sheath velocity is zero. Panel **(b)** shows the magnitude of B_y plotted in the x-z plane (jet flow in the $+x$ direction indicated by the large arrow) at the center of the simulation box, $y = 100\Delta$ at simulation time $t = 70\,\omega_{pe}^{-1}$ for the case of $\gamma_j = 15$ and $m_i/m_e = 1836$. This panel covers one-fifth of the whole simulation system. The arrows show the magnetic field in the plane.


Fig. 2. Electric and magnetic field generated by a relativistic electron ion jet core with $\gamma_j = 15$ and stationary sheath plasma for the case with the mass ratio $m_i/me = 1836$. The magnitude of E_z is plotted in the y-z plane (jet flow is out of the page) at the center of the simulation box, at $x = 500\Delta$ at $t = 30\omega_{pe}^{-1}$ **(a)**. Panel **(b)** shows E_z (blue), E_x (black), and E_y (red) at $x = 500\Delta$ and $y = 100\Delta$ at the same time. Since the magnetic field grows more slowly (see Fig. 4), panel **(c)** shows B_y (red), B_x (black), and B_z (blue) at $t = 70\omega_{pe}^{-1}$.

2.2 Core-sheath jet KKHI results

Our new simulation results using the real mass ratio are shown to compare with our previous results (Nishikawa et al., 2013).

Figure 1b shows the magnitude of B_y plotted in the x-z plane (jet flow in the $+x$ direction indicated by the large arrow) at the center of the simulation box, $y = 100\Delta$ at simulation time $t = 70\,\omega_{pe}^{-1}$ for the case of $\gamma_j = 15$ and $m_i/m_e = 1836$.

Figure 2a shows the magnitude of E_z plotted in the y-z plane (jet flow is out of the page) at the center of the simulation box, $x = 500\Delta$ at $t = 30\,\omega_{pe}^{-1}$. Figure 2b shows E_z (blue), E_x (black), and E_y (red) electric field components at $x = 500\Delta$ and $y = 100\Delta$ at time $t = 30\,\omega_{pe}^{-1}$. As shown in Fig. 4, the z component of electric field, E_z grows quickly, this DC electric field is shown in Figs. 2a and b. As expected, the y component of magnetic field, B_y is very small at this earlier time. The magnetic field grows later. Figure 2c shows B_y (red), B_x (black), and B_z (blue) magnetic field components at $x = 500\Delta$ and $y = 100\Delta$ $t = 70\,\omega_{pe}^{-1}$.
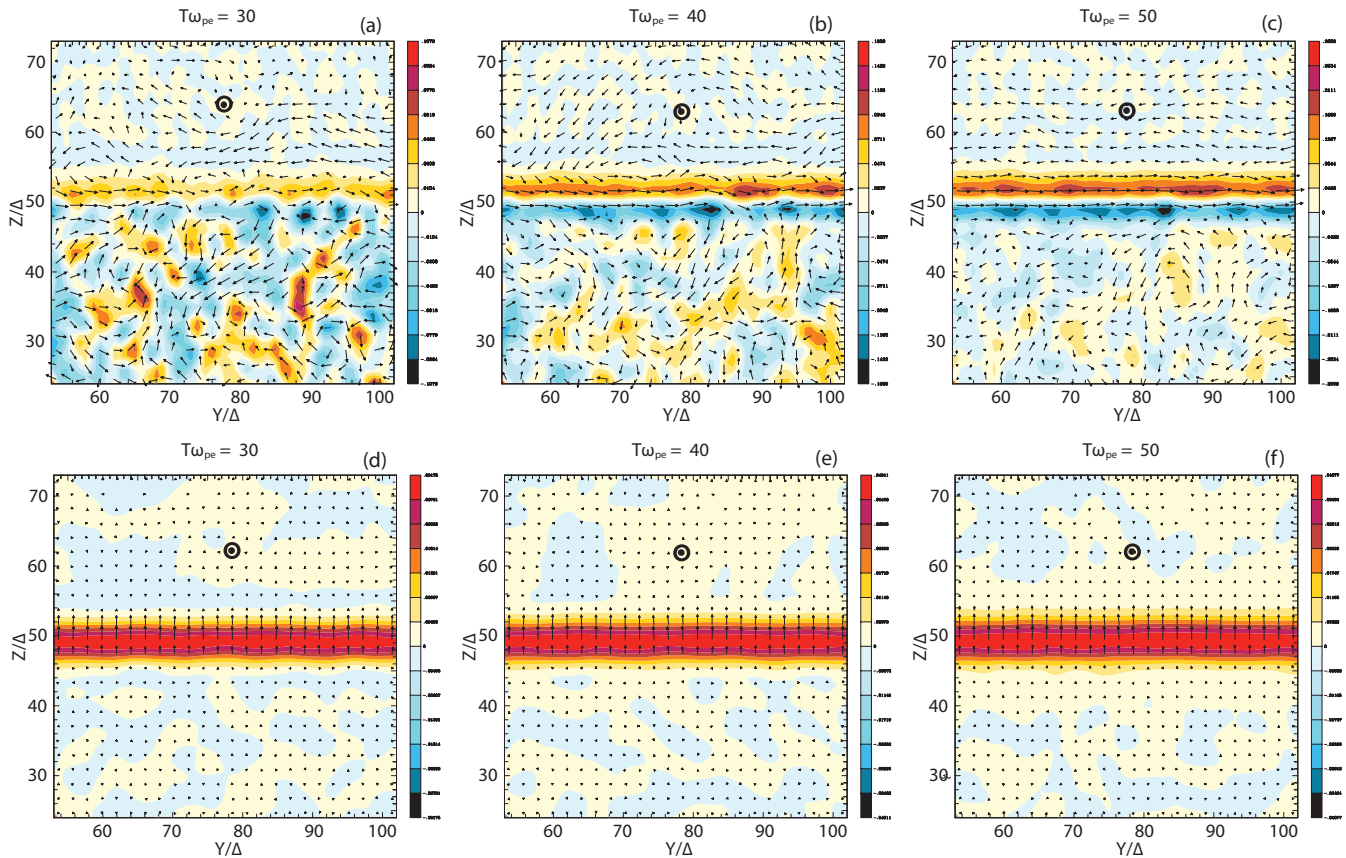
Fig. 3. The time evolution of current filaments (J_x) and electric field (E_z) in the area denoted by the small box in Fig. 2a. KKHI starts to grow at **(a)** $t = 30\omega_{pe}^{-1}$ and current filaments become large but have not yet merged by **(c)** $t = 50\omega_{pe}^{-1}$. The maximum current density (simulation units) is **(a)** ± 0.108 at $t = 30\omega_{pe}^{-1}$, **(b)** ± 0.166 at $t = 40\omega_{pe}^{-1}$, and **(c)** ± 0.296 at $t = 50\omega_{pe}^{-1}$. The arrows show the magnetic field (B_y, B_z) (the length of the arrows are not scaled to the strength of the magnetic fields). Panels **(d)**, **(e)**, and **(f)** show the time evolution of the electric field (E_z) in the same area as the current filaments. The rather uniform electric field grows even at $t = 30\omega_{pe}^{-1}$. The maximum values of E_z change with time **(d)** ± 0.032, **(e)** ± 0.040, and **(f)** ± 0.040. As seen from green lines in Fig. 4a, electric fields achieve a maximum at $t = 45\omega_{pe}^{-1}$ and subsequently decrease.

Figure 3 shows the evolution of current filaments along the jet (J_x) and the z component of the electric field (E_z) at an earlier time. Jet flow out of the page is indicated by $\odot$. Current filaments inside the jet ($z/\Delta > 50$) have positive J_x and outside the current filaments have negative J_x. The width of both positive and negative current filaments is about 2–3 electron Debye lengths. This suggests that the jet electrons near the velocity shear move out of the jet slightly and/or the sheath electrons are dragged by the jet. The steady current filaments at the velocity shear create a steady E_z component. This electric field component decreases after $t = 50\omega_{pe}^{-1}$. These current filaments create a B_y component which has been reported on in the previous work (Nishikawa et al., 2013).

We have compared the differences between cases with mass ratios $m_i/m_e = 20$ and 1836 for the relativistic jet with $\gamma_j = 15$. We find that the structure and growth rate of kinetic KHI is very similar (see Fig. 4). The heavier ions in the real

mass ratio case keep the system thermal fluctuations smaller, but the kinetic KHI grows similarly. The magnetic field energy becomes larger than the electric field energy at a similar time in both cases around $t = 87\,\omega_{pe}^{-1}$. We also performed a simulation with $\gamma_j = 1.5$ and $m_i/m_e = 20$. For this non-relativistic case the magnetic field grows earlier and overtakes the electric field energy at $t = 46\,\omega_{pe}^{-1}$.

Figure 5 shows the evolution of electric and magnetic field energy for the core jet with $\gamma_j = 15$ and stationary sheath plasma for mass ratio $m_i/me = 1836$. Figure 5a shows the evolution of the total electric field energy (black), E_y (green), E_x (red), and E_x (blue). The z component grows first as shown in Fig. 3 and the y component of the magnetic field grows as shown in Fig. 5b. After B_y grows an induced electric field E_x grows as indicated by the red line in Fig. 5a. It should be noted that the magnetic field grows at a slower rate than a counter-streaming case with $\gamma_0 = 3.0$. At $t = 170\omega_{pe}^{-1}$, saturation has not yet occurred. This may be due our highly
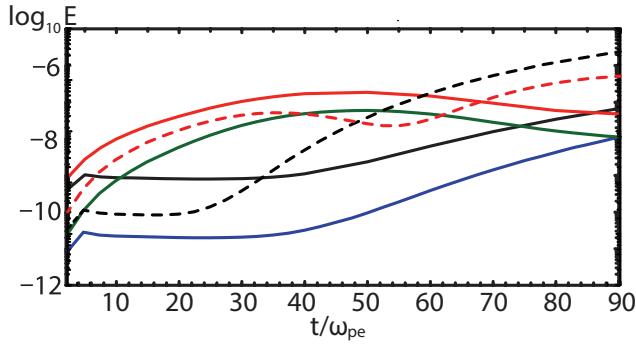
Fig. 4. The panel shows the time evolution of electric field energy (red) and magnetic field energy (black) for $\gamma_j = 15$ and $m_i/m_e = 20$ (Nishikawa et al., 2013). For the case with the real mass ratio the green and blue lines shows the time evolution of electric field energy and magnetic field energy, respectively. The dashed red and black lines show the time evolution of electric field energy and magnetic field energy, respectively for the case with $\gamma_j = 1.5$ and $m_i/m_e = 20$. For all cases the kinetic KHI grows quickly, the magnetic field energy plateaus, and later gradually grows again. In the non-relativistic case the magnetic field energy becomes larger than the electric field energy at an earlier time.

relativistic jet core resulting in a larger Lorentz factor in the "electrostatic" relativistic jet plasma frequency and larger electron inertia in the simulation frame.

3 Core-sheath dispersion relation

We have extended the analysis presented in Gruzinov (2008) to core-sheath electron-proton plasma flows, allowing for different core and sheath electron densities n_{jt} and n_{am}, respectively, and core and sheath electron velocities v_{jt} and v_{am}, respectively. In this analysis the protons are considered to be free-streaming, whereas the electron fluid quantities and fields are linearly perturbed. We consider electrostatic modes along the jet. The dispersion relation becomes

$$
\begin{aligned}
&(k^2 c^2 + \gamma_{am}^2 \omega_{p,am}^2 - \omega^2)^{1/2} (\omega - k V_{am})^2 \\
&\times [(\omega - k V_{jt})^2 - \omega_{p,jt}^2] \\
&+ (k^2 c^2 + \gamma_{jt}^2 \omega_{p,jt}^2 - \omega^2)^{1/2} (\omega - k V_{jt})^2 \\
&\times [(\omega - k V_{am})^2 - \omega_{p,am}^2] = 0,
\end{aligned}
\tag{1}
$$

where $\omega_{p,jt}$ and $\omega_{p,am}$ are the plasma frequencies ($\omega_p^2 \equiv 4\pi n e^2 / \gamma^3 m_e$) of jet and ambient electrons, respectively, $k = k_x$ is the wave number parallel to the jet flow, and γ_{jt} and γ_{am} are Lorentz factors of jet and ambient electrons, respectively.

Analytic solutions to Eq. (1) are not available except in the low ($\omega \ll \omega_p$ and $kc \ll \omega_p$) and high ($\omega \gg \omega_p$ and $kc \gg \omega_p$) frequency and wavenumber limits. In the high wavenumber limit with $V_{am} = 0$, the real frequency becomes $\omega \simeq k V_{jt} \pm \omega_{p,jt}/\sqrt{2}$. In the low wavenumber limit an analytic solution

to the dispersion relation is expressed as follows:

$$
\begin{aligned}
\omega &\simeq \frac{(\gamma_{am}\omega_{p,jt} k V_{am} + \gamma_{jt}\omega_{p,am} k V_{jt})}{(\gamma_{am}\omega_{p,jt} + \gamma_{jt}\omega_{p,am})} \\
&\pm i \frac{(\gamma_{am}\omega_{p,jt}\gamma_{jt}\omega_{p,am})^{1/2}}{(\gamma_{am}\omega_{p,jt} + \gamma_{jt}\omega_{p,am})} k(V_{jt} - V_{am}).
\end{aligned}
\tag{2}
$$

Here the real part gives the phase velocity and the imaginary part gives the temporal growth rate and directly shows the dependence of the growth rate on the velocity difference across the shear surface. Equation (2) shows that the wave speed increases and the temporal growth rate decreases as $\gamma_{jt}\omega_{p,am}/\omega_{p,jt} = \gamma_{jt}^{5/2}(n_{am}/n_{jt})^{1/2}$ increases.

We show exact solutions to Eq. (2) in Fig. (6) for a test case using the parameters, $n_{jt} = n_{am} = 0.1\,\mathrm{cm}^{-3}$, $V_{jt}/c = 0.979796$ with $\gamma_{jt} = 5.0$, and $V_{am} = 0$. Note that the number densities are determined in their proper frames. In the ambient observer frame the jet's number density would appear to be $n'_{jt} = \gamma_{jt}n_{jt} = 0.5\,\mathrm{cm}^{-3}$. With the number densities determined in the proper frames the plasma frequencies are $\omega_{p,jt} = (4\pi n_{jt}e^2/\gamma_{jt}^3 m_e)^{1/2} = 1.60 \times 10^3\,\mathrm{rad\,s}^{-1}$ and $\omega_{p,am} = (4\pi n_{am}e^2/\gamma_{am}^3 m_e)^{1/2} = 1.78 \times 10^4\,\mathrm{rad\,s}^{-1}$. At small and large wavenumbers the numerical solutions follow the analytic low and high wavenumber solutions almost exactly. The maximum temporal growth rate and associated wavenumber found from the numerical solutions shown in Fig. 6 are $\omega_I^{max} \simeq 0.93\omega_{p,jt}$ at $k^{max}c \simeq 7.0\omega_{p,jt}$ or $k^{max}V_{jt} \simeq 6.9\omega_{p,jt}$.

If we assume that $\omega_I^{max} \sim \omega_{p,jt}$ then we can use the imaginary part of Eq. (2) to estimate the wavenumber at which temporal growth is a maximum with result that we estimate $k^{max}V_{jt} \sim 7.6\omega_{p,jt}$ and these estimates are within 10% of the exact numerical solution. The low wavenumber solution, Eq. (2), provides excellent estimates of the complex frequency to wavenumbers within a factor of 2 of the maximally growing wavenumber.

4 Summary and discussion

We have investigated generation of magnetic fields associated with velocity shear between an unmagnetized relativistic jet and an unmagnetized sheath plasma (core jet-sheath configuration). We have examined the evolution of electric and magnetic fields generated by kinetic shear (Kelvin-Helmholtz) instabilities. Compared to the previous studies using counter-streaming performed by Alves et al. (2012), the structure of KKHI of our jet-sheath configuration is slightly different even for the global evolution of the strong transverse magnetic field. We find that the major components of growing modes are E_z and B_y. After the B_y component is excited, the induced electric field E_x becomes larger. However, other components are very small. We find that the structure and growth rate with $m_i/m_e = 1836$ and $m_i/m_e = 20$ are similar. In our core-sheath simulations no saturation at
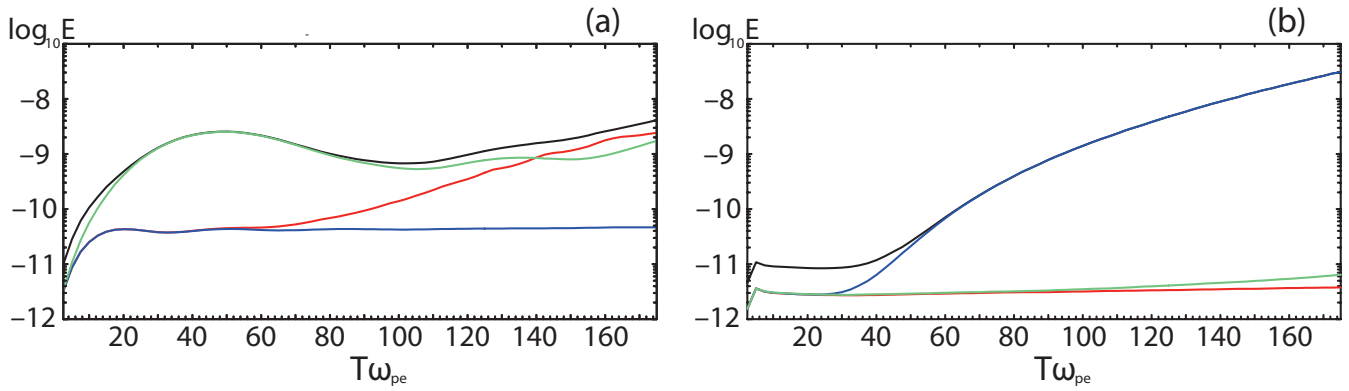
Fig. 5. Evolution of electric **(a)** and magnetic **(b)** field energies for the core jet with with $\gamma_j = 15$ and stationary sheath plasma for the case with the mass ration $m_i/me = 1836$. Panel **(a)** shows the evolution of the total electric field energy (black), E_z (green), E_x (red), and E_y (blue). The evolution of the total magnetic field energy (black), B_y (blue), B_z (green), and B_x (red) is plotted in panel **(b)**.
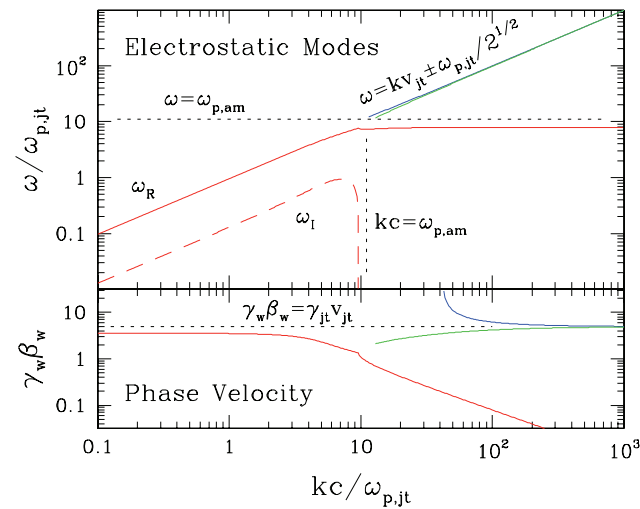
Fig. 6. The upper panel shows electrostatic mode solutions as a function of wavenumber, k, parallel to the flow direction. The real part, ω_R, and imaginary part, ω_I, of the frequency are indicated by the solid and dashed lines, respectively. The lower panel shows the phase velocity, $\gamma_w \beta_w$, where $\beta_w = \omega_R/kc$.

the later time is seen as in the counter-streaming cases. This difference seems come from that fact that the jet is highly relativistic and our simulation is done in a core-sheath configuration. The growth rate for the mildly relativistic jet case ($\gamma_j = 1.5$) is larger than the relativistic jet case ($\gamma_j = 15$).

We have calculated, self-consistently, the radiation from electrons accelerated in the turbulent magnetic fields in the relativistic shocks. We found that the synthetic spectra depend on the Lorentz factor of the jet, the jet's thermal temperature, and the strength of the generated magnetic fields (Nishikawa et al., 2011, 2012). In forthcoming work we will obtain synthetic spectra from particles accelerated by KKHI as we have done for shock simulations (Nishikawa et al., 2011, 2012).

References

Alves, E. P., Grismayer, T., Martins, S. F., Fiúza, F., Fonseca, R. A., and Silva, L. O.: Large-scale magnetic field generation via the Kelvin-Helmholtz instability in unmagnetized scenarios, ApJ, 746, L14, doi:10.1088/2041-8205/746/2/L14, 2012.

Buneman, O.: TRISTAN The D Electromagnetic Particle Code, in: Computer Space Plasma Physics: Simulation Techniques and Software, edited by: Matsumoto, H. and Omura, Y., Terra Scientific Publishing Company, Tokyo, Japan, 67–84, 1993.

Frederiksen, J. T., Haugbølle, T., Medvedev, M. V., and Nordlund, Å.: Radiation Spectral Synthesis of Relativistic Filamentation, ApJL, 722, L114–L119, 2010.

Giannios, D., Uzdensky, D. A., and Begelman, M. C.: Fast TeV variability in blazars: jets in a jet, MNRAS, 395, L29–L33, 2009.

Gruzinov, A.: GRB: magnetic fields, cosmic rays, and emission from first principles?, arXiv:0803.1182, 2008.

Liang, E., Boettcher, M., and Smith, I.: Magnetic Field Generation and Particle Energization at Relativistic Shear Boundaries in Collisionless Electron-Positron Plasmas, ApJL, 766, L19, 2013.

Martins, J. L., Martins, S. F., Fonseca, R. A., and Silva, L. O.: Radiation post-processing in PIC codes, Proc. SPIE, 7359, 73590V-1–8, 2009.

Mizuno, Y., Hardee, P., and Nishikawa, K.-I.: Relativistic Magnetohydrodynamic Simulations of Magnetized Spine-Sheath Relativistic Jets, ApJ, 662, 835–850, 2007.

Nakar, E.: Short-hard gamma-ray bursts, Phys. Reports, 442, 166–236, 2007.

Nishikawa, K.-I., Hardee, P., Richardson, G., Preece, R., Sol, H., and Fishman, G. J.: Particle Acceleration and Magnetic Field Generation in Electron-Positron Relativistic Shocks, ApJ, 622, 927–937, 2005.

Nishikawa, K.-I., Mizuno, Y., Fishman, G. J., and Hardee, P.: Particle Acceleration, Magnetic Field Generation, and Associated Emission in Collisionless Relativistic Jets, IJMP D, 17, 1761–1767, 2008.

Nishikawa, K.-I., Niemiec, J., Hardee, P. Medvedev, M., Sol, H., Mizuno, Y., Zhang, B., Pohl, M., Oka, M., and Hartmann, D. H.: Weibel instability and associated strong fields in a fully 3D simulation of a relativistic shock, ApJL, 698, L10–L13, 2009a.

Nishikawa, K.-I., Niemiec, J., Sol, H., Medvedev, M., Zhang, B., Nordlund, A., Frederiksen, J. T., Hardee, P., Mizuno, Y., Hartmann, D. H., and Fishman, G. J.: New Relativistic Particle-In-Cell Simulation Studies of Prompt and Early Afterglows from GRBs, AIPCP, 1085, 589–593, 2009b.

Nishikawa, K.-I., Niemiec, J., Medvedev, M., Zhang, B., Hardee, P., Mizuno, Y., Nordlund, Å. Frederiksen, J., Sol, H., Pohl, M., Hartmann, D. H., Oka, M., and Fishman, J. F.: Radiation from Relativistic Shocks with Turbulent Magnetic Fields, IJMP D, 19, 715–721, 2010.

Nishikawa, K.-I., Niemiec, J., Medvedev, M., Zhang, B., Hardee, P., Nordlund, Å., Frederiksen, J., Mizuno, Y., Sol, H., Pohl, M., Hartmann, D. H., Oka, M., and Fishman, J. F.: Radiation from relativistic shocks in turbulent magnetic fields, Adv. Space Res., 47, 1434–1440, 2011.

Nishikawa, K.-I., Niemiec, J., Zhang, B., Medvedev, M., Hardee, P., Mizuno, Y., Nordlund, Å., Frederiksen, J., Sol, H., Pohl, M., Hartmann, D. H., and Fishman, J. F.: Simulation of relativistic jets and associated self-consistent radiation, IJMP: Conference Series, 8, 259–264, 2012.

Nishikawa, K.-I., Hardee, P., Zhang, B., Dutan, I., Medvedev, M., Choi, E. J., Min, K. W., Niemiec, J., Mizuno, Y., Nordlund, Å. Frederiksen, J., Sol, H., Pohl, M., and Hartmann, D. H.: Radiation from accelerated particles in relativistic jets with shock, shear-flow, and re-connection, 2012 Fermi Symposium proceedings – eConf C121028, arXiv:1303.2569, 2013.

Sironi, L. and Spitkovsky, A.: Synthetic spectra from particle-in.cell simulations of relativistic collisionless shocks, ApJL, 707, L92–L96, 2009.

Zhang, W., MacFadyen, A., and Wang, P.: Three-Dimensional Relativistic Magnetohydrodynamic Simulations of the Kelvin–Helmholtz Instability: Magnetic Field Amplification by a Turbulent Dynamo, ApJL, 692, L40–L44, 2009.